

Air-Water and Water Projections in Hydraulic Jumps

Y. Chachereau¹ and H. Chanson¹

¹School of Civil Engineering
 The University of Queensland, Brisbane 4072, Australia

Abstract

A hydraulic jump is the rapid transition from a high-velocity supercritical flow to a subcritical flow. In the present study, the free-surface fluctuations and air-water flow properties were investigated in a large size facility with Reynolds numbers between 6×10^4 and 1.5×10^5 . In the highly aerated roller, the microscopic two-phase flow structure was complex. The findings highlighted the complicated interactions between the local two-phase flow properties and the free-surface deformations.

Introduction

A hydraulic jump is the rapid and sudden transition from a high-velocity supercritical open channel flow to a subcritical flow (Fig. 1). Hydraulic jumps are commonly experienced in rivers and canals, in industrial applications and in manufacturing processes [4, 11]. Figure 1 show a hydraulic jump in a culvert inlet. The discharge per unit width was about $3 \text{ m}^2/\text{s}$ corresponding to a Reynolds number of 3×10^6 . A key feature is the fluctuating nature of the free-surface and the strong aeration of the flow [5, 10]. In the highly aerated flow, the microscopic two-phase flow structure is complex, and consists of a wide range of entities including air-water projections, foam, and complicated air-water imbrications.

The present study aims to examine accurately the free surface turbulent motion and air-water flow properties in hydraulic jumps with relatively small Froude numbers ($2.4 < Fr_1 < 5.1$) operating at relatively large Reynolds numbers ($6 \times 10^4 < Re < 1.5 \times 10^5$).



Figure 1. Hydraulic jump in a culvert inlet and details of the roller free-surface - $Re \sim 3 \times 10^6$, Shutter speed: 1/80s, Flow from left to right.

Experimental Facility and Instrumentation

The experiments were performed in a horizontal rectangular flume, 3.2 m long, 0.5 m wide and 0.45 m high. The sidewalls were made of glass and the channel bed was PVC. The inflow conditions were controlled by a vertical gate with a semi-circular shape and its opening was fixed at $h = 0.036 \text{ m}$.

The water discharge was measured with a Venturi meter located in the supply line and which was calibrated on-site. The discharge measurement was accurate within $\pm 2\%$. The clear-water flow depths were measured using rail mounted point gages with a 0.2 mm accuracy. The pressure and velocity measurements in steady supercritical flows were performed with a Prandtl-Pitot tube ($\varnothing = 3.3 \text{ mm}$). The instantaneous free surface elevations were measured using ultrasonic displacement meters Microsonic™ Mic+25/IU/TC located along and above the flume centreline. The sensors had a 0.18 mm accuracy and 50 ms response time. The air-water flow properties were measured with a double-tip phase-detection probe. The dual-tip probe was equipped with two identical sensors with an inner diameter of 0.25 mm. The distance between probe tips was $\Delta x_{tip} = 7.12 \text{ mm}$. The probe was excited by an electronic system (Ref. UQ82.518) designed with a response time of less than $10 \mu\text{s}$. During the experiments, each probe sensor was sampled at 20 kHz for 45 s. The displacement and the position of the probe in the vertical direction were controlled by a fine adjustment system connected to a Mitutoyo™ digimatic scale unit with a vertical accuracy of less than 0.1 mm. Further details on the experimental apparatus and results were reported in [1].

Experimental flow conditions

Two series of experiments were conducted (Table 1). The first series focused on the general hydraulic jump properties with inflow Froude numbers between 2.4 and 5.1. In the second series, some air-water flow measurements at the sub-millimetric scale were conducted using the double-tip conductivity probe. The flow conditions corresponded to Froude numbers between 3.1 and 5.1. For both series, the jump toe was located at $x = x_1 = 1.50 \text{ m}$ where x is the longitudinal distance from the upstream gate and the same upstream rounded gate opening $h = 0.036 \text{ m}$. For these conditions, the inflow depth d_1 ranged from 0.042 down to 0.038 m depending upon the flow rate. The Pitot tube velocity data showed that the supercritical inflow was characterised by a partially-developed boundary layer ($\delta/d_1 = 0.12$ to 0.4).

Q m ³ /s	d ₁ m	Fr ₁ $\frac{V_1}{\sqrt{g \times d_1}}$	Re $\frac{V_1 \times d_1}{\nu}$	Study
0.033 to 0.0627	0.045 to 0.038	2.4 to 5.1	6.6×10^4 to 1.3×10^5	Free-surface measurements
0.0446 to 0.0627	0.044 to 0.0395	3.1 to 5.1	8.9×10^4 to 1.3×10^5	Two-phase flow measurements

Table 1. Experimental flow conditions.

Free-Surface Properties

Presentation

Downstream of the jump toe, the free surface of the hydraulic jump was strongly turbulent. Some large vertical fluctuations, foamy air-water structures and water projections were observed

for $Fr_1 > 2.3$ where Fr_1 is the upstream Froude number. The hydraulic jump was a breaking jump with air entrainment, and some projections of water droplets were observed. Visually the rate of air entrainment and air-water projections increased with increasing Froude number. A number of high-shutter speed photographs of air-water projections were taken (Fig. 2). The observations highlighted a broad range of water and air-water droplet projections immediately above the jump toe, as well as some instantaneous discontinuity of the impingement perimeter. The short-lived structures exhibited a wide range of shapes. Figure 2 shows some high-shutter speed photographs aimed to illustrate the variety of short-lived air-water structures projected above the hydraulic jump. Some large air-water structures were projected more than $5 \times d_1$ above the upstream water surface. While a large proportion of air-water structures were projected upwards with an initially forward motion, some were ejected in the negative direction, sometimes landing upstream of the jump toe. Note further in Figure 2 the water surface discontinuity at the impingement perimeter.



(A) $d_1 = 0.0395$ m, $x_1 = 1.50$ m, $Fr_1 = 5.1$, $Re = 1.2 \times 10^5$ - Shutter: 1/180 s at f/2.5, ISO 100



(B) $d_1 = 0.0395$ m, $x_1 = 1.5$ m, $Fr_1 = 5.1$, $Re = 1.3 \times 10^5$ - Shutter: 1/180 s at f/2.5, ISO 100

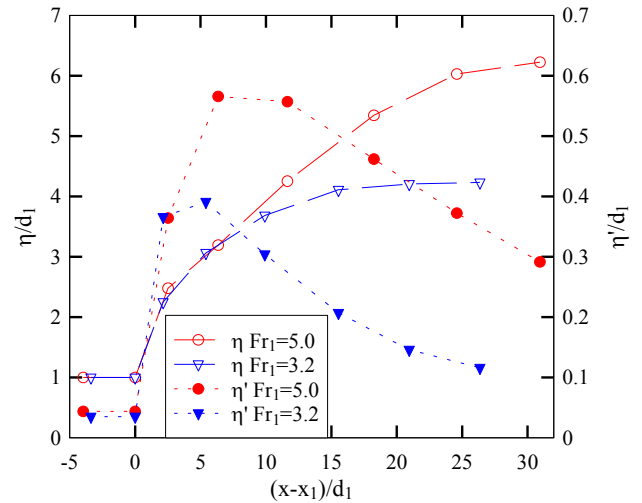
Figure 2. High-shutter speed photographs of air-water projections in hydraulic jumps, looking downstream at the impingement point and free-surface discontinuity at the jump toe - Flow from foreground to background.

Free-surface fluctuations

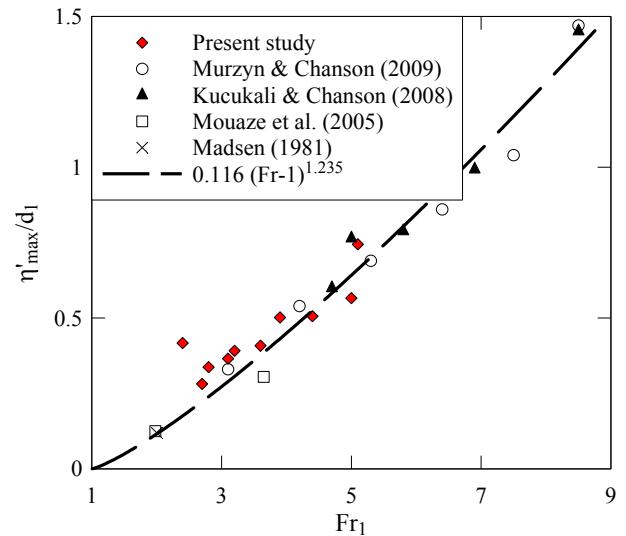
The time-averaged longitudinal free surface profiles were recorded for inflow Froude numbers ranging from 2.4 to 5.1 (Table 1). Figure 3A presents some typical profiles where η is the time-averaged water depth and η' is the standard deviation of the free-surface elevation. The data showed that the time-averaged longitudinal profiles were very close to the

photographic observations through the glass sidewalls. Some small free-surface fluctuations were observed upstream of the jump toe ($x < x_1$). A significant increase in free surface fluctuation was observed immediately downstream of the jump toe for all Froude numbers, and the free-surface fluctuations reached a maximum value η'_{max} within the first half of the roller (Fig. 2A). Further downstream, the free-surface fluctuations η' decreased with increasing distance from the jump toe. The results were consistent with earlier studies [8, 9].

The peak in turbulent fluctuations was observed for $(x-x_1)/d_1 < 7$. For $Fr_1 = 2.7$, η'_{max} was about $0.3 \times d_1$, while it was $0.7 \times d_1$ for $Fr_1 = 5.1$. This maximum value η'_{max} increased with increasing Froude numbers (Fig. 3B). The large standard deviations in free-surface elevations were linked with a large number of air-water projections above the roller and jump toe seen in Figure 2. Note that, with the present experimental setup, an increasing Froude number was associated with an increasing Reynolds number. The present data were compared with the data fit proposed by Murzyn and Chanson [9]:

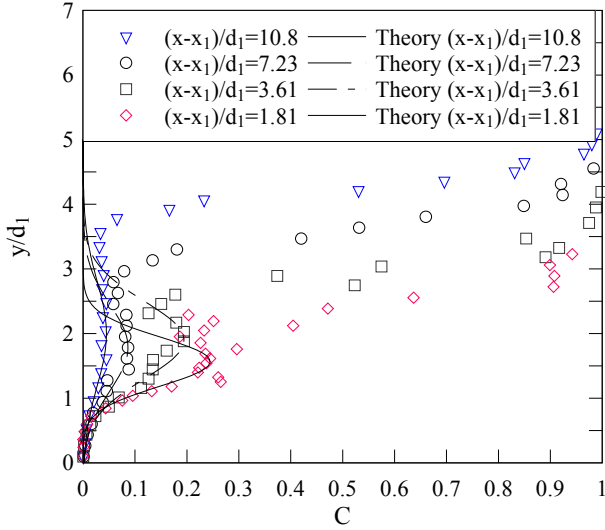


(A) Dimensionless longitudinal profiles of time-averaged water elevation η/d_1 and free surface fluctuations η'/d_1 in a hydraulic jump for $Fr_1 = 3.2$ and 5.1

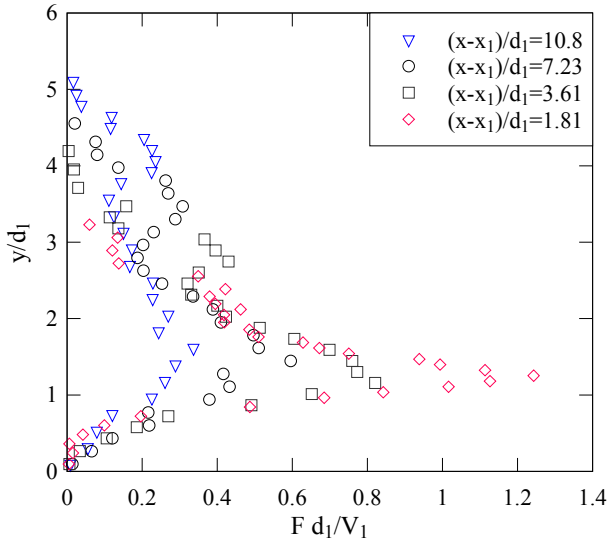


(B) Maximum of turbulent fluctuations η'_{max}/d_1 in hydraulic jumps as a function of Froude number Fr_1 - Comparison between experimental data and Equation (1).

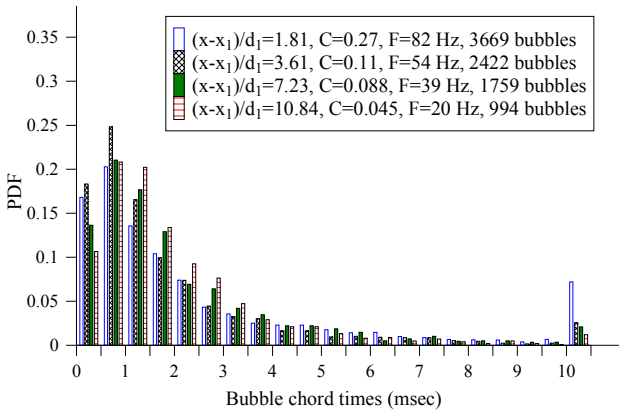
Figure 3. Free-surface properties of hydraulic jumps.



(A) Void fraction distributions.



(B) Bubble count distributions.



(C) Bubble chord time distributions where $F = F_{\max}$.

Figure 4. Two-phase flow properties in the air-water shear layer. $Fr_1 = 3.8$, $Re = 0.8 \times 10^4$, $d_1 = 0.0405$ m, $x_1 = 1.50$ m.

$$\left(\frac{\eta'}{d_1}\right)_{\max} = 0.116(Fr_1 - 1)^{1.235} \quad (1)$$

Equation (1) is compared with experimental data in Figure 3B.

Two-Phase Flow Properties

The breaking hydraulic jumps were characterised by some significant air bubble entrainment and intense turbulence, thus resulting in a complex two-phase flow. In the hydraulic jump roller, two distinct air-water flow regions were identified: the lower region dominated by a developing turbulent shear layer; and the upper part consisting in the free surface region characterised by large void fraction, splashes and recirculation areas. In the air-water shear layer, the void fraction reached a local maximum, while the void fraction profiles were compared successfully with an analytical solution of the advective diffusion equation for air bubble in a uniform flow [2]:

$$C = C_{\max} \exp\left(-\frac{\left(\frac{y - y_{C_{\max}}}{d_1}\right)^2}{4D^{\#}\left(\frac{x - x_1}{d_1}\right)}\right) \quad (2)$$

where C_{\max} is the maximum void fraction in the shear layer, located at the vertical elevation $y_{C_{\max}}$, $D^{\#}$ is the dimensionless turbulent diffusivity. Figure 4A presents some typical void fraction profiles at different longitudinal locations for $Fr_1 = 3.8$, and the data are compared with Equation (2).

The bubble count rate F was defined as the number of air bubbles detected by the conductivity probe leading tip per unit time at a given location (x, y) . Figure 4B presents some typical vertical distributions of dimensionless bubble count rates for $Fr_1 = 3.8$. The data highlighted a maximum bubble count rate in the air-water shear layer.

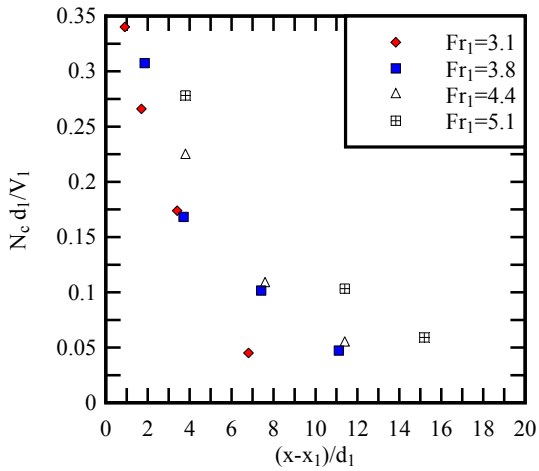
While the metrology could not measure directly the bubble sizes, the probe output provided the bubble chord time defined as the time spent by the bubble on the probe tip. Figure 4C presents some probability distribution functions of bubble chord times at the elevation where the bubble count rate was maximum for $Fr_1 = 3.8$. The experimental data showed a broad spectrum of chord times at the investigated locations. The bubble chord times measured ranged from less than 0.5 ms to more than 10 ms. The chord times smaller than 2 ms were clearly predominant in every case with the largest probability between 0.5 and 1 ms.

Bubble clustering

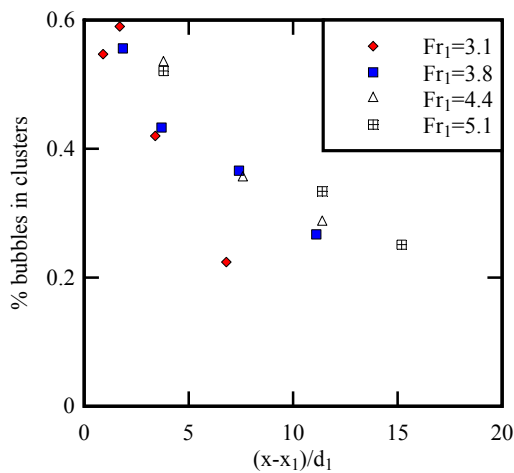
The entrained bubbles interacted with the turbulence structures, yielding to some turbulent dissipation and the formation of bubble clusters [3]. In hydraulic jumps, the clustering index may provide a measure of the vorticity production rate, of the level of bubble-turbulence interactions and of the associated energy dissipation. The longitudinal structure of the air-water flow was analysed and two bubbles were considered parts of a cluster when the water chord time between two consecutive bubbles was less than the bubble chord time of the lead particle. That is, when a bubble was in the near-wake of the leading particle. The criterion was based upon a comparison between the local, instantaneous characteristic flow times.

The experimental results showed systematically a number of trends. The number of clusters per second N_c was substantial in the air-water shear layer, and decreased rapidly with increasing longitudinal distance (Fig. 5A). A large proportion of bubbles were parts of a cluster structure in the air-water shear zone. That is, up to half of all bubbles in the beginning of the shear layer ($(x-x_1)/d_1 < 5$), and the percentage of bubbles in clusters decreased with increasing longitudinal distance (Fig. 5B). In average, the number of bubbles per cluster ranged from 2.7 down to 2.3 and decreased with increasing distance from the jump toe (Fig. 5C).

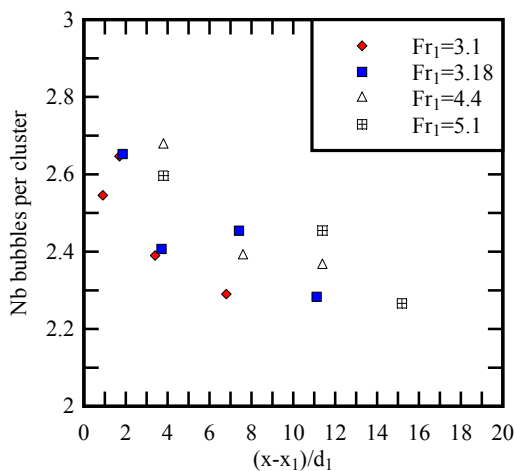
In a cluster, the lead bubble was followed by a group of bubbles. The data showed that the lead bubble chord was larger in average than the typical cluster bubble chord; the ratio of lead bubble chord to mean cluster bubble chord ranged from 1.4 down to 1.15, decreasing with increasing distance from the jump toe [1].



(A) Dimensionless number of cluster per second $N_c d_1 / V_1$.



(B) Percentage of bubbles in clusters.



(C) Number of bubbles per cluster structure.

Figure 5. Characteristic properties of bubble clusters in the air-water shear layer at the locations where $F = F_{max}$.

Conclusion

The hydraulic jump is a complex phenomenon that remains incompletely understood. In the present study, both the free surface fluctuations and the air-water properties were investigated experimentally in hydraulic jumps with relatively small Froude numbers between 2.4 and 5.1 and relatively large Reynolds numbers ($6 \times 10^4 < Re < 1.5 \times 10^5$). The shape of the mean free surface profile was well defined and in agreement with visual observations. The turbulent fluctuation profiles exhibited a peak of maximum intensity in the first half of the hydraulic jump roller that reflected the large number of air-water projections above the roller free-surface. The air-water flow measurements highlighted two characteristic regions: the air-water shear layer and an upper free-surface region above. The air-water shear zone was characterised by local maxima in terms of void fraction and bubble count rate. The probability distribution functions (PDF) of bubble chord time showed that the bubble chord times exhibited a broad spectrum. An analysis of the longitudinal air-water structure highlighted a significant proportion of bubbles travelling within a cluster structure.

References

- [1] Chachereau, Y., and Chanson, H., (2010). Free-Surface Turbulent Fluctuations and Air-Water Flow Measurements in Hydraulic Jumps with Small Inflow Froude Numbers. *Hydraulic Model Report No. CH78/10*, School of Civil Eng, University of Queensland, Brisbane, Australia, 138 pages.
- [2] Chanson, H. (1997). *Air Bubble Entrainment in Free-Surface Turbulent Shear Flows*. Academic Press, London, UK, 401 pages.
- [3] Chanson, H. (2007). Bubbly Flow Structure in Hydraulic Jump. *Eur. JI of Mechanics B/Fluids*, Vol. 26, No. 3, pp.367-384.
- [4] Chanson, H. (2009). Current Knowledge In Hydraulic Jumps And Related Phenomena. A Survey of Experimental Results. *Eur. JI of Mechanics B/Fluids*, Vol. 28, No. 2, pp. 191-210.
- [5] Chanson, H., and Brattberg, T. (2000). Experimental Study of the Air-Water Shear Flow in a Hydraulic Jump. *Intl JI of Multiphase Flow*, Vol. 26, No. 4, pp. 583-607.
- [6] Kucukali, S., and Chanson, H. (2008). Turbulence Measurements in Hydraulic Jumps with Partially-Developed Inflow Conditions. *Exp. Thermal and Fluid Science*, Vol. 33, No. 1, pp. 41-53.
- [7] Madsen, P.A. (1981). A Model for a Turbulent Bore. *Ph.D. thesis*, Tech. Univ. of Denmark, Inst. of Hydrodynamics and Hyd. Eng., Copenhagen, Denmark, 149 pages.
- [8] Mouazé, D., Murzyn, F., and Chaplin, J.R. (2005). Free Surface Length Scale Estimation in Hydraulic Jumps. *Jl of Fluids Eng., Trans. ASME*, Vol. 127, pp. 1191-1193.
- [9] Murzyn, F., and Chanson, H. (2009). Free-Surface Fluctuations in Hydraulic Jumps: Experimental Observations. *Exp. Thermal and Fluid Science*, Vol. 33, No. 7, pp. 1055-1064.
- [10] Murzyn, F., Mouazé, D., and Chaplin, J.R. (2005). Optical Fibre Probe Measurements of Bubbly Flow in Hydraulic Jumps. *Intl JI of Multiphase Flow*, Vol. 31, No. 1, pp. 141-154.
- [11] Rajaratnam, N. (1967). Hydraulic Jumps. *Advances in Hydrosience*, Ed. V.T. Chow, Academic Press, New York, USA, Vol. 4, pp. 197-280..